Available online at www.sciencedirect.com

SciVerse ScienceDirect

Ceramics International 39 (2013) 6607–6610

CERAMICS INTERNATIONAL

www.elsevier.com/locate/ceramint

Synthesis and characterization of CeO_2 nano-rods

Yong Chen[a,b], Tianmo Liu[a,*], Chunlin Chen[b], Weiwei Guo[a], Rong Sun[c], Shuhui Lv[b], Mitsuhiro Saito[b], Susumu Tsukimoto[b], Zhongchang Wang[b]

[a]*College of Materials Science and Engineering, Chongqing University, Chongqing 400044, PR China*
[b]*WPI Research Center, Advanced Institute for Materials Research, Tohoku University, 2-1-1 Katahira, Aoba-ku, Sendai, Japan*
[c]*Institute of Engineering Innovation, The University of Tokyo, 2-11-16 Yayoi, Bunkyo-ku, Tokyo 113-8656, Japan*

Received 16 January 2013; received in revised form 28 January 2013; accepted 28 January 2013
Available online 4 February 2013

Abstract

We report a synthesis of two types of CeO_2 nano-rods *via* the facile and efficient hydrothermal process free from any surfactant and template. The synthesized nano-rods are chemically identified as CeO_2 with the standard fluorite structure but their morphologies are different. The nano-rods prepared with cerium nitrate hexahydrate and sodium phosphate are thicker and shorter with diameter of ~30 nm and length of ~100 nm, and those prepared with cerium acetate hydrate and dibasic sodium phosphate are thinner and longer with ~10 nm in diameter and ~400 nm in length. Microstructural analyses reveal that the two species of nano-rods have low-energy {111} surfaces and grow along the ⟨112⟩ direction. As a consequence of their morphologies, the two types of synthesized nano-rods exhibit excellent UV-absorption ability in comparison to the irregular CeO_2 nanoparticles.

Keywords: B. Microstructure; D. CeO_2; Hydrothermal process; Nano-rods; UV absorption

1. Introduction

As one of the most reactive rare-earth metal oxides, ceria (CeO_2) has attracted extensive attention recently due to the hope it raises for many technological applications in a wide range of fields. The three-way catalysts, oxygen sensors, solid fuel cells, and UV blockers are just a few representative examples [1–5]. To date, a number of methods have been developed for the synthesis of nanostructured CeO_2, involving high-intensity ultrasound, rapid microwave, and hydrothermal process [6–9]. Of all these methods, the hydrothermal technique is gaining increasing popularity owing to many of its intrinsic merits such as one step, low temperature, simple operation, low energy consumption, and the possibility for large-scale industrialization [10].

For most of the applications, morphology of CeO_2 is widely recognized as a key to modifying its chemical and physical properties due to surface effect. Extensive efforts have therefore been devoted over past decades to morphology control of nanostructured CeO_2 so as to meet practical demands. Up to now, a wide range of CeO_2 nanostructures with tunable shape or size have been successfully synthesized, including the nano-cubes, nano-octahedrons, nano-spheres and other hybrid architectures [11–16]. Among all of the CeO_2 morphologies, one-dimensional (1D) structure is of strong interest because its unique physical properties, which are not expected in its bulk constituent, are promising for many potential technological applications [17]. Here, two species of 1D nano-rods of CeO_2 are fabricated *via* a facile hydrothermal process. Morphology of the nano-rods is characterized systematically, based on which a growth mechanism of the nano-rods is proposed.

2. Experimental

All chemical reagents were of analytical grade (Sigma-Aldrich Co. Ltd.) and used with no further purification. Two types of CeO_2 nano-rods were prepared by the hydrothermal method. One is fabricated by first dissolving cerium nitrate hexahydrate ($Ce(NO_3)_3 \cdot 6H_2O$) and sodium phosphate (Na_3PO_4) in distilled water (40 mL) under an

*Corresponding author. Tel.: +86 81222175933.
E-mail addresses: chenyongjsnt@yahoo.com.cn (Y. Chen), tmliu@cqu.edu.cn (T. Liu), zcwang@wpi-aimr.tohoku.ac.jp (Z. Wang).

0272-8842/$ - see front matter © 2013 Elsevier Ltd and Techna Group S.r.l. All rights reserved.
http://dx.doi.org/10.1016/j.ceramint.2013.01.096

intensive stirring for 15 min (called type-I sample hereafter). H_2O_2 was then dropped into the solution under strong stirring for 30 min to produce the precursor. The relative molar ratio among $Ce(NO_3)_3$, Na_3PO_4 and H_2O_2 is fixed to 1:0.01:0.006. Next, the solution was transferred into autoclaves and treated at 230 °C for 24 h under autogenous pressure. White products were eventually obtained by centrifuging, washing with distilled water and ethanol to remove unwanted ions, and drying at 60 °C in air. The other type of sample was prepared by dissolving cerium acetate hydrate ($Ce(Ac)_3 \cdot nH_2O$) and dibasic sodium phosphate (Na_2HPO_4) in distilled water with no further addition of H_2O_2 (called type-II sample hereafter). The relative molar ratio of cerium acetate hydrate ($Ce(Ac)_3 \cdot nH_2O$) to dibasic sodium phosphate (Na_2HPO_4) is adopted to be 1:0.01. To make comparison, nanoparticles were also prepared by dissolving $Ce(NO_3)_3 \cdot 6H_2O$ (3 mmol) and ammonium acetate (CH_3COONH_4) of 2 mmol into distilled water, followed instantly by stirring for 15 min. The polyethylene glycol (PEG) was then dropped into the solution. The solution was finally transferred to the autoclave and treated at 200 °C for 24 h under autogenous pressure. Microstructural analyses were performed using the x-ray diffraction (XRD), scanning electron microscopy (SEM) and transmission electron microscopy (TEM). For the XRD, a Rigaku D/Max-1200X diffractometry with the Cu Kα radiation operated at 30 kV and 100 mA was used. Surface morphologies were observed using the Hitachi SU 8000 SEM. Crystal structures were observed by the TEM (JEM-2010F, JEOL Co. Ltd.) operated at an accelerating voltage of 200 kV. The UV-shielding properties were examined with an UV–vis spectrophotometer.

3. Results and discussion

Typical XRD spectra of the two as-prepared samples are shown in Fig. 1, where the above pattern belongs to the type-I sample and the lower one is the type-II sample. The diffraction patterns of the two samples are indexed as CeO_2 with a fluorite structure. No diffraction peaks of any other cerium-based impurities are detected, which indicates that the synthesized samples are composed of fluorite-type ceria alone. Fig. 2(a)–(d) presents field-emission SEM micrographs of the as-synthesized CeO_2, which reveal a rod-like morphology for the two samples. However, the nano-rods are thicker and shorter in the type-I sample (Fig. 2(a) and (b)) than in the type-II sample (Fig. 2(c) and (d)). That is, the nano-rods in the type-I sample have an average diameter of ~30 nm and an average length of ~100 nm, and the nano-rods in the type-II sample exhibit an average diameter of ~10 nm and an average length of ~400 nm. To shed light on growth mechanism of the nano-rods, TEM observations are performed for the type-II sample (Fig. 2(e)) because the morphology and crystal structure are similar in the two samples. The nano-rods are uniform with a diameter of ~10 nm and a length of several hundreds of nanometers, judging from the bright-field TEM image. Fig. 2(g) shows an enlarged TEM image of an individual CeO_2 nano-rod, which indicates a good crystallinity for the CeO_2 nano-rods.

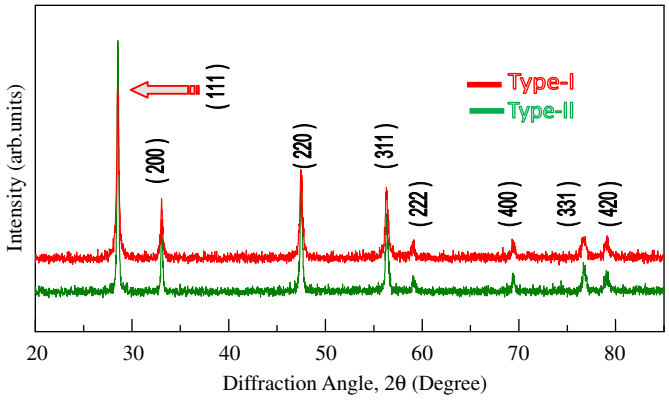

Fig. 1. XRD spectra of the two species of CeO_2 nano-rods synthesized with different chemical reagents.

The high-resolution (HRTEM) images provided further aimed at clarifying the growth mechanism of the CeO_2 nano-rods. From Fig. 2(g), the interplanar distance of the CeO_2 lattice fringes parallel to the surface of the nano-rod is determined to be 0.314 nm, in accord with the distance between the {111} crystal planes in the fluorite-type ceria. This suggests that surface of the nano-rods is along the {111} crystal planes of CeO_2. Fig. 2(h) presents a fast Fourier transform (FFT) of the HRTEM image, from which the zone axis is determined to be the [110] direction. Further comparison of Fig. 2(g) with (h) uncovers that the longitudinal direction of the CeO_2 nano-rods is $(\bar{2}24)$, indicating that the nano-rods grow along the $\langle 112 \rangle$ direction.

Fig. 3 illustrates schematically the evolution process of the nano-rods. Since the Na_3PO_4 aqueous solution is strongly alkaline, the following hydrolysis is predominant:

$$Na_3PO_4 + 2H_2O \rightarrow 3Na^+ + 2OH^- + (HPO_4)^{2-}. \quad (1)$$

In contrast, the Na_2HPO_4 solution is weakly alkaline, which slows down the hydrolysis reaction process, as can be expressed by the following equation:

$$Na_2HPO_4 + 2H_2O \rightarrow 3Na^+ + 2OH^- + H_2PO_4^-. \quad (2)$$

When $Ce(NO_3)_3 \cdot 6H_2O$ and Na_3PO_4 are taken as chemical reagents, the Ce^{3+} cations, which are produced by the dissolution of $Ce(NO_3)_3 \cdot 6H_2O$, first react with OH^- anions coming from the hydrolysis of Na_3PO_4 (Eq. (1)). This process results in precipitation of the milky $Ce(OH)_3 \cdot nH_2O$ (Eq. (3)). The as-prepared $Ce(OH)_3 \cdot nH_2O$ is oxidized instantly to $CeO_2 \cdot nH_2O$ after the drop of H_2O_2, which generates oxygen (Eq. (4)). Since the Na_3PO_4 hydrolysis takes place very quickly, a large amount of OH^- anions are produced instantly (Eq. (1)), which induces reactions (3) and (4) immediately. As a result of these reactions, a vast amount of $CeO_2 \cdot nH_2O$ precursors are obtained in short time. $CeO_2 \cdot nH_2O$ precursors therefore

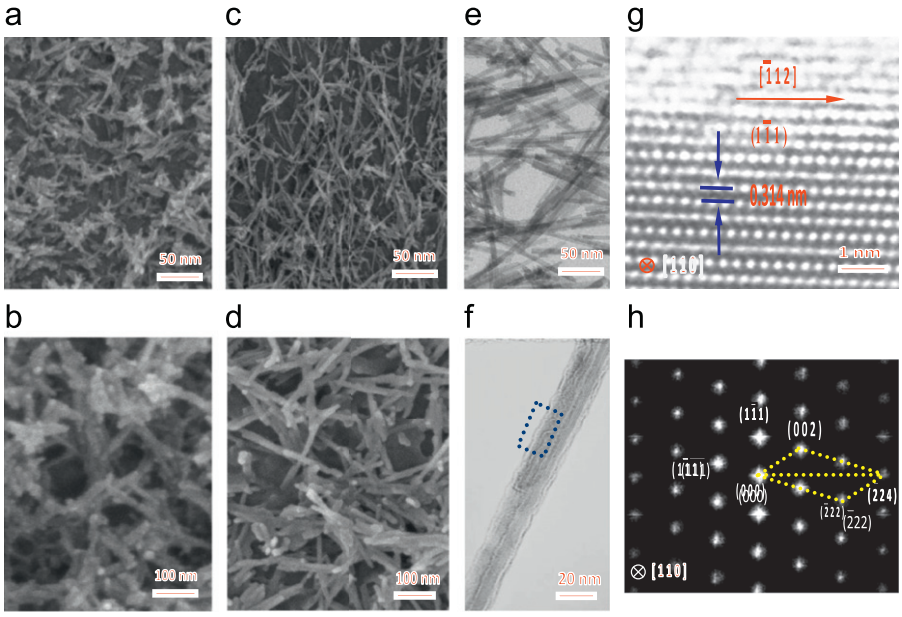

Fig. 2. (a) and (b) SEM images revealing the nano-rods in the type-I sample. (c) and (d) Corresponding SEM images of the type-II sample. (e) TEM image of the nano-rods in the type-II sample. (f) TEM image showing an individual nano-rod in the type-II sample. (g) HRTEM image taken over the area square marked in (f). (h) Fast Fourier transform of the HRTEM image shown in (g).

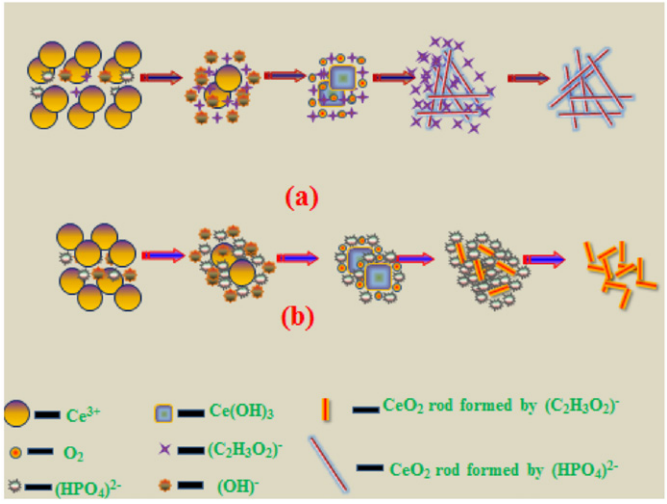

Fig. 3. Schematic illustration of the evolution process of the nano-rods prepared with (a) $Ce(Ac)_3$ and Na_2HPO_4, and (b) $Ce(NO_3)_3$, Na_3PO_4 and H_2O_2.

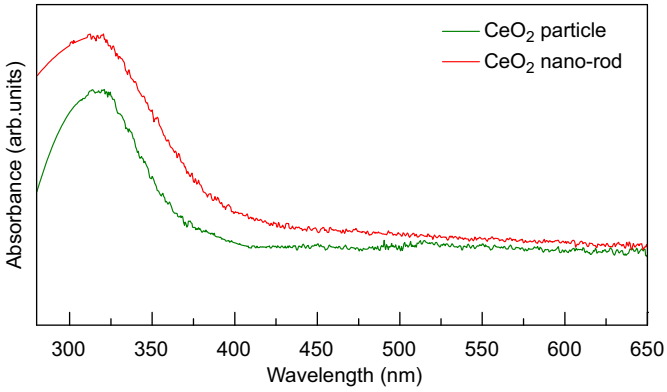

Fig. 4. UV–vis absorption spectra of the CeO_2 nano-rods in the type-II sample. The absorption spectrum of the nanoparticles prepared with $Ce(NO_3)_3 \cdot 6H_2O$, CH_3COONH_4, and PEG are given as well for a straightforward comparison.

cannot reach equilibrium condition during growth, giving rise to comparable growth rate along diameter and length direction. This forms the coarse and short morphology for the nano-rods.

On the other hand, when the $Ce(Ac)_3 \cdot nH_2O$ and Na_2HPO_4 are applied as chemical reagents, the concentration of OH^- is very low in the solution due to the slow hydrolysis of Na_2HPO_4, which drives reaction (3) to occur slowly. In view of the fact that no H_2O_2 is added and that the oxygen solubility in liquid solution is low, the oxidation of $Ce(OH)_3 \cdot nH_2O$ (Eq. (4)) (i.e., an oxygen consuming process) should slow down as well. In this case, all the reactions are dynamically slow, leading to the possibility that the growth of CeO_2 nano-rods can reach equilibrium conditions. As a result, surfaces of the nano-rods are exposed with the low-index and low-energy {111} planes, which explains the observed thinner and longer nano-rods in the type-II sample

$$Ce^{3+} + 3OH^- + nH_2O \rightarrow Ce(OH)_3 \cdot nH_2O \quad (3)$$

$$4Ce(OH)_3 \cdot nH_2O + O_2 \rightarrow 4CeO_2 \cdot nH_2O + 4H_3O^+ + 2O^{2-} \quad (4)$$

Fig. 4 presents UV–vis absorption spectra of the CeO_2 nano-rods together with that of the irregular CeO_2 nanoparticles as a reference [18]. The highest absorbance peak for the nanoparticles and nano-rods appears at wavelength

of 320 and 310 nm, respectively. In addition, a strong absorption band emerges at UV range of 270–340 nm, which may originate from the charge transfer between the O 2p and Ce 4f states [19]. Evidently, the UV absorption range is wider for the nano-rods than that of nanoparticles. Since it is generally believed that a good UV-shielding material should hold the ability to absorb the UV ray with a wavelength of less than 400 nm [20], our prepared CeO_2 nano-rods may act as an efficient UV-shielding candidate.

Summing up, two species of fluorite-type CeO_2 nano-rods with different sizes are fabricated through a simple yet efficient hydrothermal method using different chemical reagents. Surfaces of the nano-rods are determined to be along the {111} planes and the nano-rod growth direction is along the ⟨112⟩ direction. Moreover, the nano-rods in the two types of samples present different morphologies with diameter of ~30 nm and length of ~100 nm for the type-I sample, and diameter of ~10 nm and length of ~400 nm for the type-II sample. The prepared nano-rods exhibit a wider range of UV absorption than that of the nanoparticles.

Acknowledgments

Y.C. appreciates the Chinese Scholarship Council (CSC) for financial support. Z.W. thanks financial supports from the Grant-in-Aid for Young Scientists (A) (Grant no. 24686069) and the Challenging Exploratory Research (Grant no. 24656376).

References

[1] J.P. Nair, E. Wachtel, I. Lubomirsky, J. Fleig, J. Maier, Anomalous expansion of CeO_2 nanocrystalline membranes, Advanced Materials 15 (2003) 2077–2081.
[2] B.C.H. Steele, A. Heinzel, Materials for fuel-cell technologies, Nature 414 (2001) 345–352.
[3] P. Jasinski, T. Suzuki, H.U. Anderson, Nanocrystalline undoped ceria oxygen sensor, Sensors and Actuators B 95 (2003) 73–77.
[4] R.D. Robinson, E.S. Jonathan, F. Zhang, Visible thermal emission from sub-band-gap laser excited cerium dioxide particles, Journal of Applied Physics 92 (2002) 1936–1941.
[5] S. Tsunekawa, T. Fukuda, A. Kasuya, Blue shift in ultraviolet absorption spectra of monodisperse CeO_{2-x} nanoparticles, Journal of Applied Physics 87 (2000) 1318–1321.
[6] H. Lian, M. Zhang, J. Liu, Z. Ye, J. Yan, C. Shi, Synthesis and spectral properties of lutetium-doped CeF_3 nanoparticles, Chemical Physics Letters 395 (2004) 362–365.
[7] W. Zeng, T.M. Liu, Z.C. Wang, Enhanced gas sensing properties by SnO_2 nanosphere functionalized TiO_2 nanobelts, Journal of Materials Chemistry 22 (2012) 3544–3548.
[8] H.Y. Jin, N. Wang, L. Xu, S. Hou, Synthesis and conductivity of cerium oxide nanoparticles, Materials Letters 64 (2010) 1254–1256.
[9] L. Ma, W.X. Chen, Z.D. Xu, Complexing reagent-assisted microwave synthesis of uniform and monodisperse disk-like CeF_3 particles, Materials Letters 62 (2008) 2596–2599.
[10] W. Zeng, T.M. Liu, Z.C. Wang, S. Tsukimoto, M. Saito, Y. Ikuhara, Selective detection of formaldehyde gas using a Cd-doped TiO_2–SnO_2 sensor, Sensors 9 (2009) 9029–9038.
[11] S. Guo, H. Arwin, S.N. Jacobsen, K. Järrendahl, U.J. Helmersson, A spectroscopic ellipsometry study of cerium dioxide thin films grown on sapphire by rf magnetron sputtering, Journal of Applied Physics 77 (1995) 5369–5376.
[12] B. Elidrissi, M. Addou, M. Regragui, C. Monty, A. Bougrine, A. Kachouane, Structural and optical properties of CeO_2 thin films prepared by spray pyrolysis, Thin Solid Films 379 (2000) 23–27.
[13] J.J. Miao, H. Wang, Y.R. Lia, J.M. Zhu, J.J. Zhu, Ultrasonic-induced synthesis of CeO_2 nanotubes, Journal of Crystal Growth 281 (2005) 525–529.
[14] I. Porqueras, C. Person, C. Corbella, M. Vives, A. Pinyol, E. Bertran, Characteristics of e-beam deposited electrochromic CeO_2 thin films, Solid State Ionics 165 (2003) 131–137.
[15] Y. Chen, T.M. Liu, C.L. Chen, R. Sun, S.L. Lv, M. Saito, S. Tsukimoto, Z.C. Wang, Facile synthesis of hybrid hexagonal CeF_3 nano-disks on CeO_2 frustum pyramids, Materials Letters 92 (2013) 7–10.
[16] P.X. Huang, F. Wu, B.L. Zhu, X.P. Gao, H.Y. Zhu, T.Y. Yan, W.P. Huang, S.H. Wu, D.Y. Song, CeO_2 nanorods and gold nanocrystals supported on CeO_2 nanorods as catalyst, Journal of Physical Chemistry B 109 (2005) 19169-1974.
[17] T. Masui, K. Fujiwara, K. Machida, G. Adachi, Characterization of cerium(IV) oxide ultrafine particles prepared using reversed micelles, Chemistry of Materials 9 (1997) 2197–2204.
[18] W. Zeng, T.M. Liu, Z.C. Wang, UV light activation of TiO_2-doped SnO_2 thick film for sensing ethanol at room temperature, Materials Transactions 51 (2010) 243–245.
[19] C. Ho, J.C. Yu, T. Kwong, A.C. Mak, S. Lai, Morphology-controllable synthesis of mesoporous CeO_2 nano- and microstructures, Chemistry of Materials 17 (2005) 4514–4522.
[20] L. Li, Y.S. Chen, Preparation of nanometer-scale CeO_2 particles via a complex thermo-decomposition method, Materials Science and Engineering A 406 (2005) 180–185.